THE JOURNAL OF PHYSICAL CHEMISTRY A

Article

pubs.acs.org/JPCA

Electronic Structure of Covalently Linked Zinc Bacteriochlorin Molecular Arrays: Insights into Molecular Design for NIR Light Harvesting

Kushal Shrestha,[†] Jessica M. González-Delgado,[‡] James H. Blew,[†] and Elena Jakubikova*[,†]

[†]Department of Chemistry, North Carolina State University, Raleigh, North Carolina 27695, United States

[‡]Department of Chemistry, University of Puerto Rico, Rio Piedras Campus, San Juan, Puerto Rico 00931, United States

Supporting Information

ABSTRACT: Pigment-based molecular arrays, especially those based on porphyrins, have been extensively studied as viable components of artificial light harvesting devices. Unlike porphyrins, bacteriochlorins absorb strongly in the NIR, yet little is known of the applicability of covalently linked bacteriochlorin-based arrays in this arena. To lay the foundation for future studies of excited state properties of such arrays, we present a systematic study of the ground state electronic structure of zinc bacteriochlorin (ZnBC) molecular arrays with various linkers and linker attachment sites (*meso* vs β) employing density functional theory in combination with the energy-based fragmentation (EBF) method, and the EBF with molecular orbitals (EBF-MO) method. We find that the level of steric hindrance between the ZnBC and the linker is directly correlated with the amount of ground sate electronic interactions between the ZnBCs. Low steric hindrance between the ZnBC and the linker found in alkyne-linked arrays results in strongly interacting arrays that are characterized by a decrease in the HOMO−LUMO energy gaps, large orbital energy dispersion in the frontier region, and low ZnBC-linker rotational barriers. In contrast, sterically hindered linkers, such as aryl-based linkers, result in weakly interacting arrays characterized by increased orbital energy degeneracy in the frontier region and high ZnBC-linker rotational barriers. For all linkers studied, the level of steric hindrance decreases when the ZnBCs are linked at the β position. Hence, ZnBC arrays that exhibit strong, weak, or intermediate ground-state electronic interactions can be realized by adjusting the level of steric hindrance with a judicious choice of the linker type and linker attachment site. Such tuning may be essential for design of light harvesting arrays with desired spectral properties.

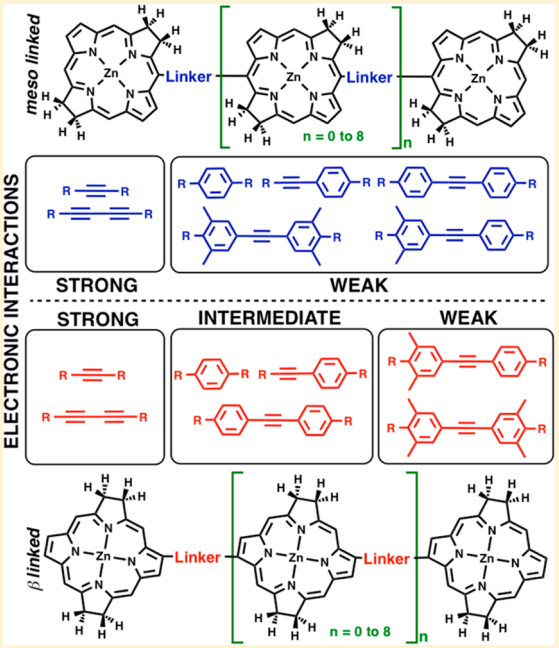

1. INTRODUCTION

Bacteriochlorins play an integral role in the natural processes of photosynthesis in bacteria. These photosynthetic systems make ample use of photons in the red and near-infrared (NIR) energy regions of the solar spectrum and employ aggregates of bacteriochlorins as the primary absorbers in light harvesting architectures.[1−4] Despite the abundance of bacteriochlorin derivatives in nature, they are underutilized in photochemical applications.[5] In contrast, porphyrins have found a wide range of applications in this field,[6−8] mainly due to the ease of synthesis of porphyrins in comparison to bacteriochlorins. In particular, covalently linked porphyrin molecular arrays have emerged as model systems for studying excitation energy and charge transfer for applications in artificial light harvesting systems and as molecular photonic wires and optoelectronic gates.[7−15]

Bacteriochlorins and porphyrins share a common macrocyclic scaffold, but they differ in the degree of the π system saturation. While porphyrins are composed of four pyrrole rings connected via four methine linkages, bacteriochlorins are characterized by two pyrrole and two pyrroline rings joined in an alternating arrangement via four methine linkages. These simple structural differences have profound consequences for ground and excited electronic properties of the two pigments. For example, porphyrins display only a weak absorption in the red and no absorption in the NIR regions of the solar spectrum, while bacteriochlorins absorb very strongly in the NIR.[16] Bacteriochlorins are also more easily oxidized and harder to

Received: August 1, 2014
Revised: September 18, 2014
Published: September 19, 2014

reduce than porphyrins and possess lower symmetry (C_{2v} vs D_{2h} for free-base porphyrins or D_{4h} for metalloporphyrins), which leads to broadening of the bacteriochlorin Soret and Q absorption bands.[17]

Artificial light harvesting molecular architectures that take advantage of energy-cascading mechanisms could clearly benefit from chromophores like bacteriochlorins that have strong absorption in the NIR.[6,13] However, little is known about the tunability of the electronic properties of extended bacteriochlorin arrays as synthesis of large, covalently linked bacteriochlorin arrays is very resource-intensive.[18] Only a handful of bacteriochlorin containing dyads have been prepared and extensively studied.[18−21] Bacteriochlorin-bacteriochlorin dimers have been synthesized through modification of naturally occurring pigments like bacteriopheophorbide *a*.[22,23] As it is difficult to isolate spectral signatures that identify one bacteriochlorin over the other in the dimers, spectroscopic studies have been aimed at understanding the excited state dynamics of chlorin-bacteriochlorin dyads.[24−26] These dyads have been synthesized by de novo routes[27−29] as well as other approaches that employ naturally derived components.[30−34]

Computational studies of bacteriochlorin-based monomers,[35,36] dimers, and oligomers are, on the other hand, very feasible and can be utilized to determine if such arrays are suitable candidates for components of artificial light harvesting architectures. In this respect, computational studies that have analyzed excitonic coupling,[37−42] charge-transfer states,[43−45] electronic response to structural modifications,[46−48] two-photon absorption,[49] and excitation energy transfer[50,51] in a variety of porphyrin-based arrays have already been instrumental in aiding our understanding of their ground and excited state electronic properties. For example, Okuno and co-workers have made large strides in elucidating the mechanism of the through-bond excitation energy transfer (EET) processes in porphyrin arrays.[52−54] The nonadiabatic interactions between the excited states of the donor and acceptor responsible for the EET in these arrays were shown to be facilitated by rotation of the donor moiety that induced increased π conjugation with the linker.[47,50,51]

Quantum chemical studies have also investigated the excited state properties of bacteriochlorin−bacteriochlorin dimers but, to date, have not tackled larger arrays.[19−21,55,56] For instance, a computational study by Head-Gordon and co-workers explored the character of low-lying charge-transfer excited states in phenylene-linked bacteriochlorin-based dyads.[21] Their work demonstrated the need for the use of long-range corrected density functionals[19,57] for proper description of charge-transfer excitation energies in these and similar molecular arrays. By contrast, ground state properties of bacteriochlorin arrays have been largely overlooked in such studies, yet they are fundamental to our understanding of the excited state processes. Moreover, our computational tools allow us to obtain the electronic structure of arrays composed of hundreds of atoms normally not accessible by standard approaches.[58]

As many of the pigment-based arrays are constructed with the intention to harvest sunlight and funnel the harvested energy into a particular site, dynamical processes of EET in such arrays are of particular interest. EET can generally be separated into through-space[59] EET (TS-EET) and through-bond[60,61] EET (TB-EET) processes. In systems that can be described by a donor-bridge-acceptor (D-B-A) model (e.g., covalently bound porphyrin arrays), the identity of the bridge plays an integral role in both TS-EET and TB-EET processes.[60−68] The bridge can affect the individual donor−acceptor transition dipoles and the donor−acceptor distance, both of which can impact the TS-EET rates.[63,65,67] The bridge and its electronic structure are also intricately connected to TB-EET. The bridge-mediated superexchange EET theory that explains TB-EET in D-B-A systems is sensitive to the electronic structure of the bridge[60,61,64,66−68] (i.e., the linker in covalently linked porphyrin arrays). Hence a deeper understanding of the role played by the linker in coupling pigment subunits in larger arrays is paramount to our ability to design bacteriochlorin arrays with desired properties.

Here we employ density functional theory (DFT) to study the ground state electronic structure of a variety of zinc bacteriochlorin (ZnBC) arrays, with ZnBC subunits covalently linked by distinct aryl- and alkyne-based linkers at the meso−meso or β−β positions (see Figure 1).

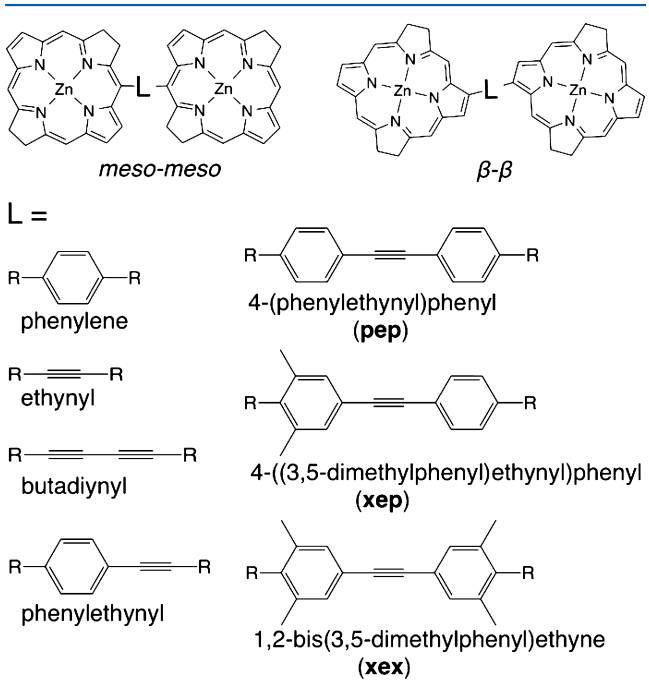

Figure 1. meso−meso and β−β Linker attachment and all linkers (represented by L) are shown.

For some linkers, we have chosen to systematically extend the arrays until they contained as many as ten ZnBC subunits. With respect to large arrays that contain several hundreds of atoms, conventional DFT and ab initio calculations are computationally intractable. Since the steep computational cost associated with electronic structure calculations of such large systems is a well-known problem, several methodologies (e.g., linear scaling approaches,[69−73] quantum mechanics and molecular mechanics combined approaches,[74−76] subsystem DFT methodologies,[77,78] and molecular fragmentation methods[79] that are density matrix-based[80−83] or energy-based[58,84−88]) that make these calculations more feasible have already been developed. We have chosen to employ an energy-based fragmentation (EBF) method[58] based on the generalized energy-based fragmentation method (GEBF),[89] the systematic molecular fragmentation method (SMF),[88] and the molecular tailoring approach (MTA)[84] in our calculations of large arrays.

Our goal is to uncover the role that the linker and linker attachment site play in modulating the electronic properties of

dx.doi.org/10.1021/jp507749c | J. Phys. Chem. A 2014, 118, 9901−9913

ZnBC arrays and to determine the linker and linker attachment sites that provide for the strongest as well as the weakest electronic interactions between the ZnBC subunits in the ground state. The insights gained in this work lay a foundation for future investigations of excited-state processes in bacteriochlorin arrays.

2. COMPUTATIONAL METHODS

Structure optimization and electronic structure calculations of ZnBC monomers and dimers were done at the B3LYP level of theory,[90,91] employing the 6-31G* basis set[92,93] for C, H, and N atoms and LANL08 effective core potential with associated basis set for Zn.[94] Gaussian 09[95] (G09) was utilized to perform all calculations on monomers and dimers. Gnuplot 4.4 plotting software and the GaussView[96] visualization program were used to generate plots and three-dimensional molecular structures contained in this work.

An EBF method[58,79,84,86−89,97−103] was employed for structure optimizations of ZnBC trimers and larger arrays. An example of the systematic fragmentation schemes utilized for the ZnBC arrays is shown in Figure S1 of the Supporting Information. The Hessians in the EBF-based optimizations were updated using the Broyden-Fletcher-Goldfard-Shanno[104] procedure. Ground state electronic structure calculations for trimers through decamers were done by means of the EBF with molecular orbitals (EBF-MO) method as described in ref 58. Single point energy calculations for all superfragments are performed with G09. Scripts written in the Python programming language postprocess the G09 output to obtain the energies, forces, Hessian matrices, and molecular orbitals of the entire system.

For systems with strong delocalization of ground state orbitals (i.e., arrays with the ethynyl group in the linker), the EBF-MO method may produce invader orbitals, which are nonphysical orbitals that sometimes invade the frontier region.[58] All invader orbitals that appear in the frontier region of the ZnBC arrays in this study were removed after visual inspection. All structure optimizations and ground state electronic structure calculations for monomers through decamers were performed in vacuum.

Potential energy surface (PES) scans were performed for all dimers in this study. One internal coordinate, specifically the dihedral angle between the ZnBC subunit and the linker, was incremented at 10° intervals, starting from the optimized value. At each step of the scan, all internal coordinates except the chosen dihedral angle were relaxed to minimize the total energy.

3. RESULTS AND DISCUSSION

In the sections that follow, results from ground state electronic structure calculations on covalently linked ZnBC dimers and larger oligomers are presented. For the sake of brevity, linker, linker attachment site, and array size information for a specific ZnBC array will be conveyed as "*meso*-linker *n*-mer" or "*β*-linker *n*-mer" (linker = phenylene, ethynyl, butadiynyl, etc., *meso* = *meso*-*meso*, *β* = *β*−*β*, and *n* = di, tri, tetra, etc.) from this point forward. A close survey of the electronic properties of the 14 ZnBC dimers reveals that they can be divided in three different groups based on the extent of the electronic interactions between the bacteriochlorin subunits: (1) strongly interacting (e.g., *β*-ethynyl, *β*-butadiynyl, *meso*-butadiynyl ZnBC dimers), (2) weakly interacting (e.g *meso*-phenylene ZnBC dimer), and (3) dimers with intermediate interaction (e.g., *β*-phenylene dimers). Therefore, only results from a representative set of six ZnBC dimers (*meso*-phenylene, *β*-phenylene, *meso*-butadiynyl, *β*-butadiynyl, *meso*-ethynyl, and *β*-ethynyl dimers) that fall into these three groups and highlight the gradient in observations from one extreme case to the other are displayed and discussed in these sections. Results for all other dimers can be found in the Supporting Information. Analogously, calculations on oligomers constructed from this representative set form the entirety of the study on larger ZnBC arrays.

3.1. Covalently Linked ZnBC Dimers.

3.1.1. Ground State Structure. Optimized geometries of dimers constructed with the linkers as shown Figure 1 were obtained: phenylene, phenylethynyl, 4-[(3,5-dimethylphenyl)ethynyl]phenyl (xep), ethynyl, butadiynyl, 1,2-bis(3,5-dimethylphenyl)ethyne (xex), and 4-(phenylethynyl)phenyl (pep). Linker-ZnBC and ZnBC−ZnBC dihedral angles at the optimized structures of the dimers are shown in Table 1.

Table 1. Linker-ZnBC and ZnBC−ZnBC Dihedral Angles for meso- and *β*-Linked Dimers

attachment site-linker	linker-ZnBC dihedral angle[a] (degrees)	ZnBC−ZnBC dihedral angle (degrees)
meso-butadiynyl	–	0.1
meso-ethynyl	–	42.7
meso-phenylethynyl	90.0	0.1
meso-xep	89.9	0.0
meso-phenylene	89.9	0.0
meso-pep	89.9	0.1
meso-xex	89.9	0.0
β-butadiynyl	–	0.2
β-ethynyl	–	0.1
β-phenylethynyl	21.3	43.3
β-xep	65.0	40.5
β-phenylene	43.4	0.1
β-pep	43.4	81.7
β-xex	89.8	0.0

[a]In dimers with aryl-based linkers, there are two possible linker-ZnBC dihedral angles. An average of the two angles is shown.

With the exception of the *meso*-ethynyl dimer, all *meso*-linked dimers display coplanar ZnBC subunits. The *meso*-ethynyl dimer, owing to increased steric crowding due to a ZnBC−ZnBC distance of 4.07 Å, has a ZnBC−ZnBC dihedral angle of 42.71° (Figure S2c of the Supporting Information). The dimers with *meso*-linked aryl-based linkers have structures in which the aryl groups are perpendicular to the subunits of ZnBC (Figure S2a of the Supporting Information).

The *β*-linked ethynyl-based dimers are in general less sterically hindered when compared to the *meso*-linked dimers. For instance, while the distance between the ZnBC subunits is virtually identical in the *β*-ethynyl and *meso*-ethynyl dimers (4.04 vs 4.07 Å), the ZnBC subunits are coplanar in the *β*-ethynyl dimer and tilted in the meso-ethynyl dimer (Figures S2c and S2d of the Supporting Information). *β*-aryl linkers also introduce less steric hindrance than the *meso*-aryl linkers. Consequently, *β*-aryl linked dimers have linker-ZnBC dihedral angles between 21° and 65°, in contrast to 90° dihedral angles in meso-aryl linked dimers. An exception to this trend is the *β*-xex dimer, with the dihedral angle of 90°. This can be explained

dx.doi.org/10.1021/jp507749c | J. Phys. Chem. A 2014, 118, 9901−9913

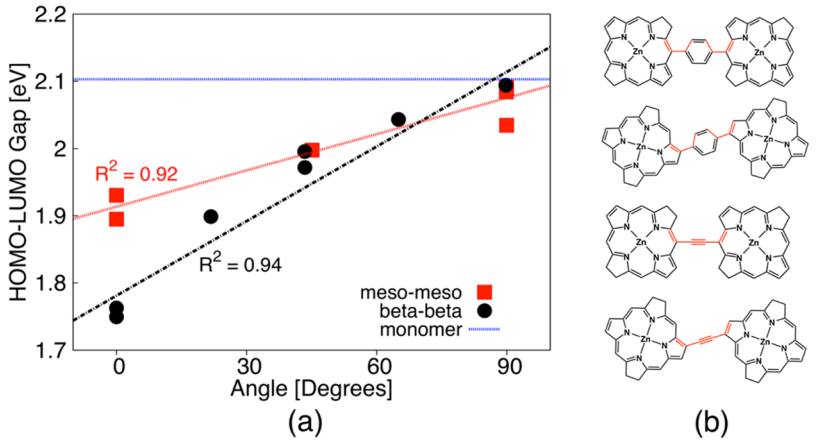

Figure 2. (a) The HOMO−LUMO gaps of the dimers are plotted against dihedral angle. The monomer HOMO−LUMO gap is shown in blue. Separate linear fits of the meso−meso linked, and $\beta-\beta$ dimers are shown. (b) The bonds that form the dihedral angle for linkers with phenyl and ethynyl groups are highlighted in red for both types of linkages. The two dihedral angles are averaged for phenyl-containing linkers.

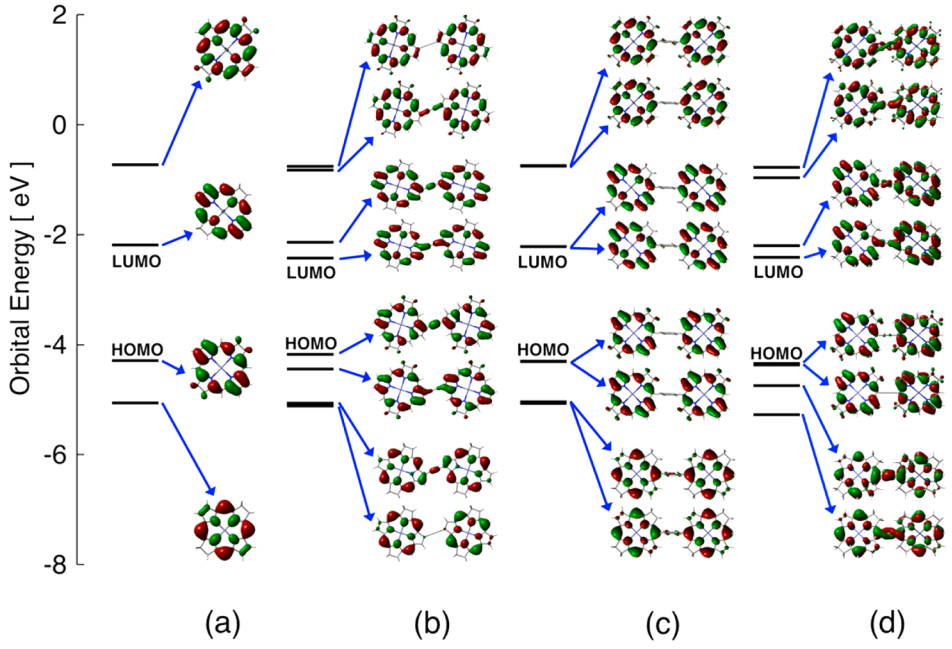

Figure 3. Energy level diagram and orbital shapes of orbitals in the frontier region for (a) the ZnBC monomer, (b) the β-ethynyl dimer, (c) the *meso*-phenylene dimer, and (d) the *meso*-ethynyl dimer. The HOMO and LUMO for each system is indicated.

by the high amount of steric hindrance provided by the 3,5-dimethyl groups on the phenyl moieties even when the linker is joined through the β-position of the two ZnBC macrocycles. Optimized structures of aryl- and alkynyl-linked dimers are shown in Figures S2 and S3 of the Supporting Information to illustrate these observations.

3.1.2. Ground State Electronic Structure. HOMO−LUMO Gaps. Structural differences introduced by the linker have a significant impact on the electronic structure of the ZnBC dimers even at 0 K. Figure 2a shows the energy difference between the highest occupied molecular orbital (HOMO) and the lowest unoccupied molecular orbital (LUMO), the HOMO−LUMO gap, of ZnBC dimers as a function of the dihedral angle between the linker and ZnBC at the optimized structure. For phenylene-, phenylethynyl-, xep-, xex-, and pep-linked dimers, there are two possible dihedral angles (highlighted in red in Figure 2b). For such cases, the average of the two angles was calculated. For the alkynyl-based linkers, the direct, dihedral angles between the ZnBC subunits were obtained (highlighted in red in Figure 2b). Linear fits of the HOMO−LUMO gaps with respect to the dihedral angles mentioned above show good linear correlations for both β- and *meso*-linked dimers with correlation coefficients (R^2) of 0.94 and 0.92, respectively. The linear correlation indicates that as the linker becomes perpendicular to the ZnBC's, the HOMO−LUMO gaps get closer to that of the monomer (shown in blue in Figure 2a).

Frontier Orbitals of Ethynyl- and Phenylene-Linked Dimers. Figure 3 shows an orbital energy level diagram for the frontier orbitals of the ZnBC monomer (Figure 3a), the β-ethynyl dimer (Figure 3b), the *meso*-phenylene dimer (Figure 3c), and the *meso*-ethynyl dimer (Figure 3d). The four orbitals from Gouterman's four-orbital model[105,106] (i.e., the two highest occupied orbitals and the two lowest unoccupied orbitals) are shown for the ZnBC monomer, while the four highest occupied and the four lowest unoccupied orbitals are

dx.doi.org/10.1021/jp507749c | J. Phys. Chem. A 2014, 118, 9901−9913

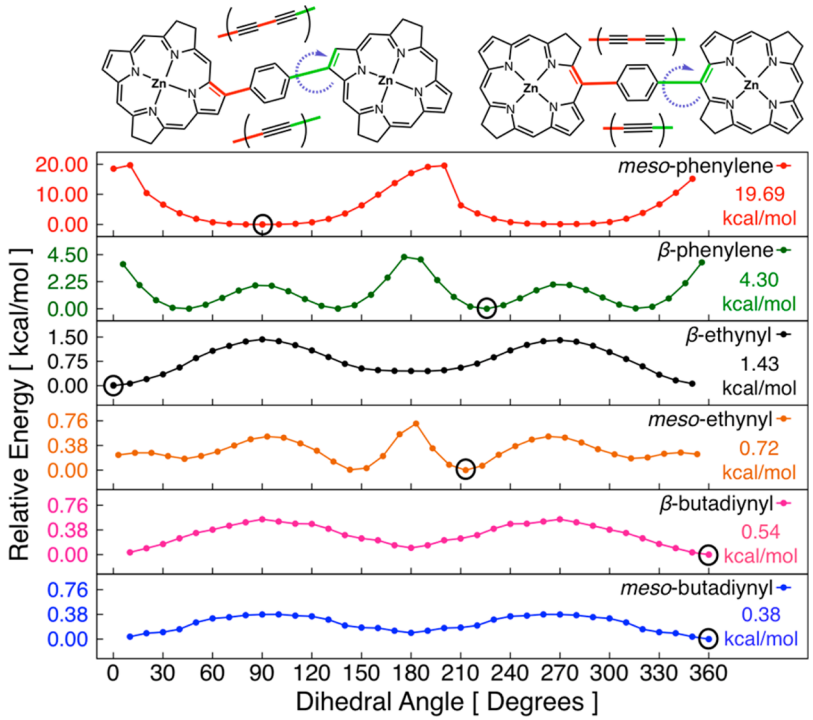

Figure 4. PES scans for rotation about the ZnBC-linker dihedral angle in covalently linked ZnBC dimers. The surfaces are labeled according to the linker and linker attachment site. The specific bond about which the ZnBC was rotated (green) is shown at the top of the figure. No rotations were made about the red bonds. The maximum for each surface is shown in kcal/mol, and the minimum on each curve is circled.

shown for the dimers. The eight orbitals of the dimers are in-phase and out-of-phase linear combinations of the four frontier orbitals of the monomer. For the *meso*-phenylene dimer (Figure 3c), all in-phase and out-of-phase linear combinations of each of the four frontier orbitals of the monomer are degenerate, resulting in four sets of degenerate orbitals.

In the case of the β-ethynyl dimer (Figure 3b), there are two sets of near-degenerate orbitals and four nondegenerate orbitals. Although the HOMO/HOMO−1 orbital pair and the LUMO/LUMO+1 orbital pair are degenerate in the *meso*-phenylene dimer, they are not degenerate in the β-ethynyl dimer. The degeneracy between LUMO and LUMO+1 is lifted as the orbital contribution from each ZnBC subunit in the β-ethynyl dimer interacts through the π system of the ethynyl linker. Similar interactions break the degeneracy in the HOMO/HOMO−1 orbital pair as well.

The near-degeneracy in the HOMO−2/HOMO−3 and the LUMO+2/LUMO+3 orbital pairs can be attributed to the lack of electron density at the β attachment site of HOMO−1 and LUMO+1 orbitals of the ZnBC monomer that combine to form HOMO−2/HOMO−3 and LUMO+2/LUMO+3 orbital pairs of the dimers. The lack of electron density at the β attachment site diminishes interactions between the ZnBC monomers and the π system of the ethynyl linker, reducing orbital energy splitting between the HOMO−2/HOMO−3 and between the LUMO+2/LUMO+3 orbital pairs.

Similarly, the four degenerate orbital pairs observed for the *meso*-phenylene dimer can be explained by the lack of any interactions between the ZnBC subunits and the π system of the phenylene linker, resulting in no orbital energy splitting among each of the four orbital pairs. The absence of orbital interactions with the phenylene π system in the case of the *meso*-phenylene dimer is facilitated by the structural orthogonality between the phenylene linker and the ZnBC subunits. Without orbital energy splitting, the four degenerate orbital pairs in the *meso*-phenylene dimer have orbital energies close to those of the four frontier orbitals of the ZnBC monomer. This accounts for the trend observed in Figure 2a.

There is only one pair of degenerate orbitals and three pairs of nondegenerate orbitals in the frontier MO region of the *meso*-ethynyl dimer (Figure 3d). The nondegenerate orbital pairs arise from orbital energy splitting between HOMO−2/HOMO−3, LUMO/LUMO+1, and LUMO+2/LUMO+3 orbitals, respectively. The HOMO/HOMO−1 orbital pair is degenerate, as the orbital contributions from each ZnBC subunit for these orbitals (HOMO of the ZnBC monomer in this case) do not have sufficient electron density at the meso position to interact with the π system of the ethynyl linker.

Overall, the degeneracy in the frontier MO region in all dimers studied herein can be explained by either the structural orthogonality between the linker and the ZnBC subunits or the lack of electron density at the linker attachment site due to the inherent symmetry of the frontier MOs of the ZnBC subunits. It may also be a combination of the two conditions.

The above explanation for the rise and lack of orbital energy splitting in the frontier region can be readily applied to all 14 dimers. Results that verify our analysis for the phenylethynyl-, xep-, xex-, and pep-linked dimers can be found in the Supporting Information.

3.1.3. Steric Hindrance and Electronic Structure. Potential Energy Surface (PES) Scans. At temperatures greater than 0 K, there exists a rotational degree of freedom about the linker-ZnBC bond for all dimers studied. The degree to which the ZnBC's can rotate about this bond is inversely related to the amount of steric hindrance introduced by the linker. PES scans were performed for all meso- and β-linked dimers with respect to the rotation around the dihedral angle between the linker and one of the ZnBC subunits. For the ethynyl- and butadiynyl

dx.doi.org/10.1021/jp507749c | J. Phys. Chem. A 2014, 118, 9901−9913

linkers, rotation around the direct dihedral angle between the two ZnBC subunits was considered.

PES scans for six select dimers are shown in Figure 4 (PES scans for all other dimers can be found in the Supporting Information). Of the six structures in Figure 4, the highest rotational energy barrier, 19.69 kcal/mol, was calculated for the *meso*-phenylene dimer, and the second-highest barrier, 4.30 kcal/mol, was calculated for the *β*-phenylene dimer. The ethynyl- and butadiynyl-linked dimers had significantly smaller rotational energy barriers that were less than 2 kcal/mol. Out of all of the dimers studied, the dimer with the highest energy barrier to rotation of 73.9 kcal/mol is the *meso*-xex dimer (the methyl substituents of the xex linker introduce a large amount of steric hindrance when the aryl moiety of this linker is forced to be coplanar to the adjacent ZnBC subunit), and the dimer with lowest energy barrier to rotation of 0.4 kcal/mol is the *meso*-butadiynyl dimer. It is important to note that rotational energy barriers obtained from the PES scans in this work serve as upper bounds to the actual energy barrier as transition state structure optimizations were not performed.

The rotational degree of freedom about the linker-ZnBC bond is an important factor to consider as such changes in the molecular structure can strongly affect the electronic structure of the ZnBC dimers. Figure 5 displays the changes in the

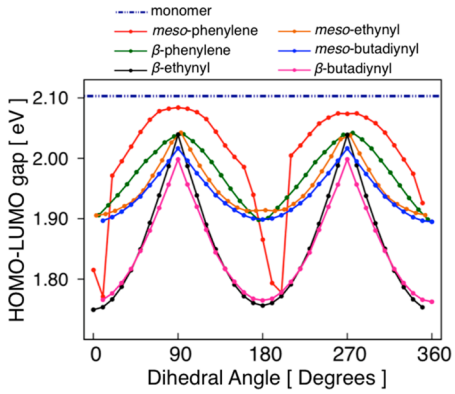

Figure 5. HOMO/LUMO orbital energy gaps of six ZnBC dimers as a function of the rotation of one ZnBC subunit. The ZnBC monomer HOMO/LUMO gap is shown for reference.

HOMO/LUMO gap as one ZnBC subunit of six select ZnBC dimers are each rotated from 0° to 360°. The trends in Figure 5 are periodic, with the HOMO/LUMO gaps reaching a minimum at coplanar conformations of the linker (or the nonrotating ZnBC subunit in the case of the butadiynyl- and ethynyl-linked dimers) and the rotating ZnBC subunit and a maximum at the corresponding perpendicular conformations. The maxima in Figure 5 occur near 90° and 270° and are at most 0.1 eV away from the HOMO/LUMO gap of the ZnBC monomer. The discontinuities that occur at around 0° and 180° in the *meso*-phenylene dimer are due to large changes in the molecular structure of the dimer upon rotation.

PES Scans and Frontier Orbitals of the β-Ethynyl Dimer. The trends observed in Figure 5 can be further elucidated by tracking the frontier orbital energies of the ZnBC dimers upon rotation. Figure 6a tracks the changes for the four lowest unoccupied and the four highest occupied orbitals of the *β*-ethynyl dimer. When the ZnBC subunits are perpendicular to one another, the four orbital pairs that arise from in-phase and out-of-phase linear combinations of the orbital contributions from each ZnBC subunit become degenerate. At these perpendicular points, the HOMO/LUMO gaps peak in magnitude and are close to the gap observed for the ZnBC monomer, which is indicative of a lack of electronic interactions.

At the optimized structure, substantial orbital energy splitting for the HOMO/HOMO−1 and LUMO/LUMO+1 orbital pairs is observed (Figure 3b). Figure 6a shows that the orbital energy splitting for both of these orbital pairs is sensitive to the rotation of one of the ZnBC subunits. The variations in the orbital energy splitting are correlated with the change in the amount of electron density on the ethynyl linker upon rotation of one of the ZnBC subunits (see Figure 6b). The LUMO and LUMO+1 become destabilized as the electron density on the linker increases. Furthermore, because the LUMO and LUMO +1 in the *β*-ethynyl dimer are respective in-phase and out-of-phase linear combinations of orbital contributions from each ZnBC subunit, when the LUMO+1 in the *β*-ethynyl dimer is stabilized, the LUMO is destabilized and vice versa. The HOMO/HOMO−1 pair also shows the same behavior. This behavior, which ultimately is evidence of strong interactions between the molecular orbitals of the ZnBC subunits and the *π* system of the linker, is the underlying cause of orbital energy splitting in all dimers.

The HOMO−2/HOMO−3 and LUMO+2/LUMO+3 orbital pairs of the *β*-ethynyl dimer show little to no orbital energy splitting upon rotation of one ZnBC subunit. The orbital energies are also relatively insensitive to the changes in the electron density on the ethynyl linker upon rotation (Figure 6). This insensitivity arises from the maintained deficiency of the electron density at the *β* positions of the ZnBC subunits due the inherent symmetry of orbital contributions from each ZnBC subunit to both the HOMO−2/HOMO−3 and LUMO +2/LUMO+3 orbital pairs. The lack of electron density at these positions significantly mutes interactions with the *π* system of the ethynyl linker, resulting in very modest to no orbital energy splitting throughout the rotation.

PES Scans and Frontier Orbitals of the meso-Phenylene Dimer. Figure 7 shows the orbital energies and the percent electron density on the linker atoms for the eight frontier orbitals of the *meso*-phenylene dimer. At the optimized molecular structure, the *meso*-phenylene dimer shows no orbital energy splitting in the frontier region (Figure 3c). Upon rotation of one ZnBC subunit into the coplanar conformation with the phenylene linker, the meso-phenylene dimer displays appreciable orbital energy splitting. It must be noted, however, that to achieve this conformation, a significant rotational energy barrier of over 19 kcal/mol must be overcome (Figure 4); therefore, the meso-phenylene dimer will very likely maintain minimal orbital interactions of the ZnBC subunit orbital contribution with the phenylene *π* system. The discontinuities that occur in the orbital energies at around 0° and 180° are due to large rearrangements in the molecular structure at these conformations.

Classification of Electronic Interactions in ZnBC Dimers. The preceding results illustrate that the molecular structure, particularly the linker and the linker attachment site, has a significant impact on the ground state electronic structure of covalently linked ZnBC dimers. Linkers and linker attachment sites that facilitate large orbital energy splitting in the frontier region result in ZnBC dimers with strong electronic interactions between the two neighboring ZnBC subunits. At the same time, strongly interacting arrays display a large

dx.doi.org/10.1021/jp507749c | J. Phys. Chem. A 2014, 118, 9901−9913

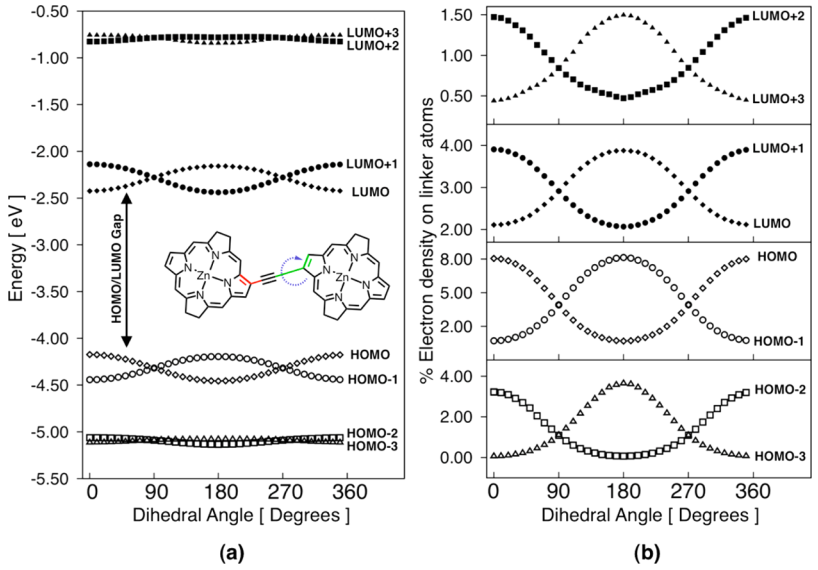

Figure 6. (a) Orbital energies of the eight frontier orbitals upon rotation of one ZnBC subunit in the *β*-ethynyl dimer. A schematic of the rotation is shown. (b) Percent electron density on the linker atoms for the eight frontier orbitals upon rotation of one ZnBC subunit in the *β*-ethynyl dimer.

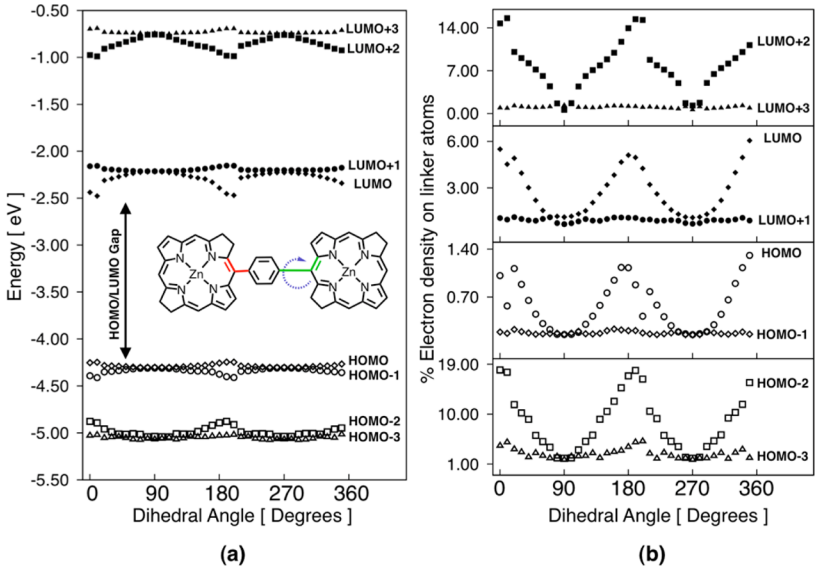

Figure 7. (a) Orbital energies of the eight frontier orbitals upon rotation of one ZnBC subunit in the *meso*-phenylene dimer. A schematic of the rotation is shown. (b) Percent electron density on the linker atoms for the eight frontier orbitals upon rotation of one ZnBC subunit in the *meso*-phenylene dimer.

amount of conformational flexibility with respect to the rotation around the linker group, and the relative orientation of ZnBC subunits (i.e., coplanar vs perpendicular) further modulates the extent of electronic interactions in the dimer.

Overall, the size of the HOMO−LUMO gap, the MO energy splitting in the frontier region (HOMO−3 − LUMO+3), and the barrier to rotation around the linker-ZnBC dihedral angles are three factors that indicate the amount of electronic interactions between the ZnBC subunits. On the basis of these properties, we have categorized each dimer considered in this study as having "strong", "intermediate", or "weak" electronic interactions between the ZnBC subunits, as shown in Table 2. In general, substantial orbital energy splitting in the frontier region (Figure 3) and a decrease in the HOMO−LUMO gap relative to that of the monomer (Figure 2) are strong indicators of electronic interactions between the ZnBC subunits in the dimer, and these factors correlate well with the barrier to rotation. Interestingly, *meso*-phenylethynyl and *β*-phenylethynyl dimers are two outliers to these trends. The *meso*-phenylethynyl dimer shows orbital energy splitting and a HOMO−LUMO gap that is comparable to that of the strongly interacting *meso*-ethynyl dimer but (unlike the *meso*-ethynyl dimer) has a high energy barrier to rotation (Table 2). The reason for the MO energy splitting and subsequent decrease in the HOMO−LUMO gap is the electronic interaction between the ethynyl linker and only one of the ZnBC subunits. Moreover, the sterically hindered phenyl group in the *meso*-phenylethynyl dimer restricts orbital interactions between the two ZnBC subunits. Therefore, the *meso*-phenylethynyl is classified as "weakly" interacting. For the same reasons, the *β*-phenylethynyl dimer is classified as having "intermediate" rather

dx.doi.org/10.1021/jp507749c | J. Phys. Chem. A 2014, 118, 9901−9913

Table 2. Rotational Barriers, HOMO-LUMO Gaps, Orbital Energy Splitting of the Frontier Orbitals, And the Level of Electronic Interactions for ZnBC Dimers[a]

attachment site-linker	rotational barrier[b] (kcal/mol)	HOMO−LUMO gap (eV)	MO splitting[c] (eV)	electronic interaction
meso-butadiynyl	0.4	1.90	0.29	strong
meso-ethynyl	0.7	1.93	0.27	strong
meso-phenylethynyl	19.1	1.93	0.18	weak
meso-xep	70.2	2.04	0.05	weak
meso-phenylene	19.7	2.08	0.01	weak
meso-pep	19.1	2.09	0.00	weak
meso-xex	73.9	2.09	0.00	weak
β-butadiynyl	0.5	1.76	0.16	strong
β-ethynyl	1.4	1.75	0.17	strong
β-phenylethynyl	4.8	1.90	0.15	intermediate
β-xep	28.7	2.05	0.03	weak
β-phenylene	4.3	1.97	0.06	intermediate
β-pep	4.8	2.00	0.04	intermediate
β-xex	29.3	2.10	0.00	weak

[a]The HOMO−LUMO gaps and MO splitting were obtained at the optimized molecular structure. [b]For dimers with more than one rotational barrier between the ZnBC and linker, the largest rotational barrier is displayed. [c]The average of the MO splitting between HOMO−3/HOMO−2, HOMO−1/HOMO, LUMO/LUMO+1, and LUMO+2/LUMO+3 orbital pairs is shown.

than "strong" electronic interactions between the ZnBC subunits.

3.2. ZnBC Oligomers. *3.2.1. Ground State Structure.* The *meso*- and *β*-phenylene, ethynyl, and butadiynyl dimers were systematically extended to include additional ZnBC's subunits. As stated previously, these six particular dimers were chosen because their properties are representative of the overall trends observed for all 14 dimers. The largest oligomers studied were decamers. The optimized structures of these larger ZnBC arrays (two examples shown in Figure S4 of the Supporting Information) are very similar to those of the dimers that were previously described (see also Figure S2 of the Supporting Information) (i.e., they display a systematic extension of the structural motifs that were present in the molecular structures of the ZnBC dimers). Vibrational analysis performed at the optimized structures of several larger arrays resulted in small imaginary frequencies (Table S1 of the Supporting Information) that correspond to very slight bending and twisting of the entire array. Considering that frequency calculations with the EBF method employed an approximate Hessian to generate the frequencies,[58] very small imaginary frequencies were expected and are considered to be negligible.

3.2.2. Electronic Structure at Ground State Optimized Geometry. The phenylene-, ethynyl-, and butadiynyl-linked extended ZnBC arrays possess the same structural features (i.e., linker types, linker attachment sites, and optimized structure motifs) as their dimer counterparts. Therefore, the effects of the molecular structure on the electronic structure of the ZnBC arrays are found to be a systematic accumulation of the effects that are observed for the dimers.

The analysis of ground state electronic structure of the *β*-ethynyl dimer shows orbital energy splitting in the frontier region (see Figure 3b). The orbital energy splitting in the frontier region is also observed in larger *β*-ethynyl oligomers. The *β*-ethynyl dimer shows two nondegenerate orbitals near both the HOMO and LUMO energies of the ZnBC monomer. Analogously, the *β*-ethynyl *n*-mers (where *n*- = tri- thru deca-) show *n* nondegenerate orbitals dispersed about the energy levels of the HOMO and LUMO of the monomer. As such, orbital energy dispersion, which is defined as the energy range covered by the nondegenerate orbitals that result from interactions with the linker *π* system, is present in the frontier region of all *β*-ethynyl oligomers (Figure 8a). The orbital energy dispersion observed for the *β*-ethynyl oligomers (Figure 8a) begins to converge to a finite value as more ZnBC subunits are added to the molecular structure. In this respect, Figure 8a demonstrates typical band formation behavior as the arrays increase in size.[48,107]

In Figure 8b, the orbitals arising from the four frontier orbitals of the ZnBC monomers in the *meso*-phenylene arrays are plotted against the number of ZnBC subunits in each array. There is little orbital energy dispersion present in all *meso*-phenylene arrays. At 0 K, all *meso*-phenylene arrays have phenylene linkers that are perpendicular to the ZnBC subunits (see Figure S4b of the Supporting Information, for example), so the interactions between the MOs of ZnBC subunits with the *π* system of the phenylene linkers are negligible. This leads to a high degree of orbital energy degeneracy in the frontier region. For instance, in the *meso*-phenylene decamer, there are four sets of degenerate orbitals that are close in energy to the four frontier orbitals of ZnBC monomer (Figure 8b), where each degenerate set contains ten orbitals. As such, unlike the *β*-ethynyl arrays, the meso-phenylene arrays are examples of arrays with weak electronic interactions, which are exemplified by little to no interaction with the *π* system of the linker.

Ground state calculations on the ZnBC arrays at 0 K indicate that (1) orbital energy splitting due to interactions between the

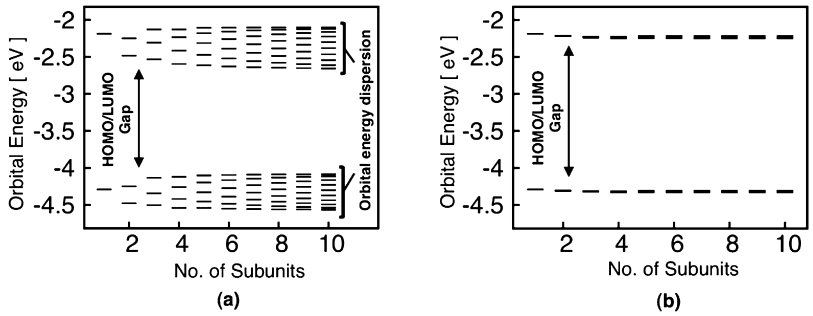

Figure 8. Orbital energy levels around the HOMO and LUMO of (a) the *β*-ethynyl- and (b) the *meso*-phenylene-linked ZnBC's arrays. The monomer HOMO and LUMO energy levels are also shown for reference. The orbital energy levels of a given array are plotted against the number of ZnBC subunits in that array. Orbital energy dispersion can be seen for the *β*-ethynyl-linked arrays.

dx.doi.org/10.1021/jp507749c | J. Phys. Chem. A 2014, 118, 9901−9913

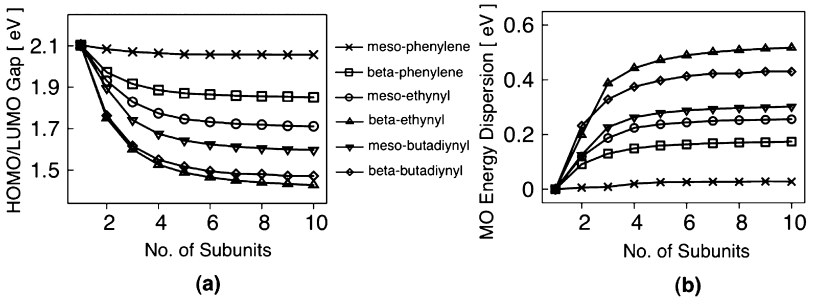

Figure 9. (a) The HOMO−LUMO gaps as a function of the number of ZnBC subunits are shown for the phenylene-, ethynyl-, and butadiynyl-linked ZnBC arrays. (b) The average of the orbital energy dispersions around the HOMO and LUMO is shown for the phenylene-, ethynyl-, and butadiynyl-linked ZnBC arrays.

ZnBC subunits that is observed in the dimer case will result in orbital energy dispersion as the dimers are systematically extended and (2) orbital energy degeneracies that were observed for the dimers will be maintained in systematically extended oligomers of any size. Hence, ZnBC arrays with a high degree of orbital dispersion in the frontier region can be categorized as arrays in which the ZnBC subunits experience strong electronic interactions. Conversely, arrays that exhibit a high degree of orbital energy degeneracy, in which the energies of the degenerate sets are close to those of the frontier orbitals of the ZnBC monomer, can be categorized as arrays with weak electronic interactions in the frontier region.

In all of the oligomers studied, orbital energy dispersion in the HOMO and LUMO regions results in the HOMO−LUMO gaps that are smaller than the HOMO−LUMO gap of the ZnBC monomer. The HOMO−LUMO gaps decrease as the arrays become longer, but the decreases eventually converge to a finite value (Figure 9a). The HOMO−LUMO orbital energy dispersion shows the inverse trend, in which the dispersion first increases, then converges to a finite value (Figure 9b). The decrease in the HOMO−LUMO gaps of the alkynyl and *β*-phenylene linked arrays is substantial as the size of the arrays increases (see Figure 9a). On the other hand, the *meso*-phenylene arrays show very little change in the energy gap upon increase in the size, and their HOMO−LUMO gaps stay close to the HOMO−LUMO gap of the monomer. The trend in the HOMO−LUMO gaps correlates with and is opposite to the trend in the amount of orbital energy dispersion around the HOMO and/or LUMO in these arrays (see Figure 9). Therefore, a decrease in the HOMO−LUMO gap of any ZnBC array is a strong indication that the array will show orbital energy dispersion around the HOMO and/or LUMO energy levels of the ZnBC monomer.

It is important to note that a decrease in the HOMO−LUMO gap alone does not indicate the overall extent of electronic interactions in the frontier region of a given array. For example, the *meso*-ethynyl arrays show smaller orbital energy dispersion near the HOMO and LUMO regions than the *β*-ethynyl arrays (Figure 9b). However, substantial orbital energy dispersion can be observed once the orbital energy range is widened to include the entire frontier region (between 0.5 and −6.0 eV, Figure 10). As a result, both *meso*- and *β*-ethynyl arrays, due to ample orbital energy dispersion in the frontier region, can be viewed as arrays with strong electronic interactions, despite the moderate decrease in the HOMO−LUMO gap of the *meso*-ethynyl arrays. Maintained degeneracy in the LUMO of all *meso*-ethynyl arrays is the reason that the HOMO−LUMO gap decreases are less pronounced.

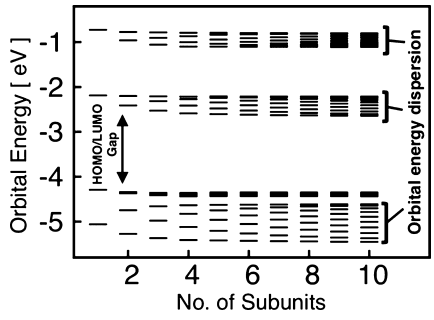

Figure 10. Orbital energy levels in the frontier energy region of *meso*-ethynyl arrays. The orbital energy levels are plotted against the number of ZnBC subunits.

3.3. Implications for Light-Harvesting and Excited State Properties. The linker and the linker attachment site strongly affect the ground state structure of covalently linked ZnBC arrays. Linkers based on aryl groups impose significant structural constraints, so the aryl groups become perpendicular to the ZnBC subunits. This is unlike phenylene-linked porphyrin oligomers in which the plane of the aryl ring is generally tilted at a 60° angle with respect to the porphyrin plane.[108] The structural orthogonality that occurs in the aryl-linked ZnBC arrays leads to a more complete canceling of electronic interactions, characterized by the orbital degeneracy in the frontier region. Furthermore, the orbital energy levels in the frontier region of arrays with weak electronic interactions have a strong resemblance to the frontier region of the ZnBC monomer (see *meso*-phenylene dimer in Figure 3c). Hence, it is likely that the electronic absorption profile of ZnBC arrays with weak electronic interactions will resemble that of the ZnBC monomer, especially for the lower energy electronic excitations, which are often confined to transitions between the MOs in the frontier region.[105,106]

Weak electronic interactions are characterized by a lack of mixing between the MOs of ZnBC subunits and the *π* system of the linker, so it is probable that arrays with weakly interacting heterogeneous subunits (e.g., some combination of bacteriochlorins, porphyrins, chlorins, perylenes, etc.) will also possess similar electronic characteristics. Molecular arrays that incorporate zinc porphyrins, free-base porphyrins, and other chromophores like perylenes that show weak electronic interactions have already been synthesized,[109] and it has been shown that their electronic absorption profile is a composite of the absorption of each chromophoric constituent of the array.[110] In a similar sense, aryl-linked ZnBC arrays with weak electronic interactions in the frontier region may show

dx.doi.org/10.1021/jp507749c | J. Phys. Chem. A 2014, 118, 9901−9913

absorption spectra that may be described as a sum of the absorption profiles of several noninteracting ZnBC monomers. Excited state studies will be necessary in order to further investigate this implication.

On the other hand, electronically interacting arrays are characterized by orbital energy dispersion in the frontier region (see Figures 8, 9, and 10). As the actual level of orbital energy dispersion varies based on the linker and linker attachment, the effects of the orbital energy dispersion on the electronic absorption profile should vary as well. Arrays that show a greater degree of orbital energy dispersion near the HOMO and LUMO display smaller HOMO−LUMO gaps (Figure 9). Such arrays will likely display strong absorptions in the NIR at energies lower than that of the ZnBC monomer. Arrays that possess a high degree of dispersion in the frontier region as a whole (e.g., the *meso*-ethynyl and *meso*-butadiynyl arrays) can be expected to show several peaks in the 350−900 nm region of the electronic absorption profile that do not exist in the ZnBC monomer. Generally, we expect that the ZnBC arrays with strong electronic interactions in the frontier region will display a larger number of low-energy transitions (see frontier region of the *meso*-ethynyl arrays in Figure 10).

With many of the arrays that exhibit strong electronic interactions, there is an additional layer of complexity when thinking about the electronic absorption profile at temperatures higher than 0 K. Linkers that introduce strong electronic interactions, mainly alkynyl-based linkers, also allow highly unhindered rotation of the ZnBC subunits about the linker-ZnBC bonds (see Figure 4). We have shown with ZnBC dimers that the rotation of the ZnBC subunits modulates the amount of orbital energy splitting, effectively coupling the ZnBC subunits at coplanar conformations and decoupling them at perpendicular conformations (see Figures 5 and 6). For such arrays, especially at room temperature, the absorption profile will likely be a sum of absorption profiles at several different conformations. It has already been shown that due to small barriers to rotation and large effects of conformation on electronic interactions, *meso*-butadiynyl porphyrin dimers exhibit different absorption spectra at coplanar and perpendicular conformations.[111−113] Therefore, similar behavior of alkynyl-linked ZnBC arrays is expected.

4. CONCLUSIONS

In this work, ground state properties and electronic structure of covalently linked ZnBC arrays connected via seven aryl- and alkyne-based linkers are investigated. The extent of electronic interactions in the ZnBC arrays is modulated both by the linker type and linker attachment site and is correlated to the amount of steric hindrance introduced by the linker. The meso attachment site is more sterically hindered, while the β attachment site facilitates stronger electronic interactions among the ZnBC subunits. In general, the aryl-based linkers at meso positions introduce significant steric hindrance and provide for minimal electronic interactions among ZnBC subunits, while the use of alkyne-based linkers at β positions results in strongly interacting ZnBC arrays. Moderate electronic interactions can be achieved with aryl-based linkers that are attached at the β positions of the ZnBC subunits. The steric hindrance is more pronounced in bacteriochlorin than in porphyrin arrays.

ZnBC arrays linked via the alkyne-based linkers possess low barriers for rotation (<1.5 kcal/mol) around the linker group and as a consequence will sample a variety of conformations at room temperature. The amount of electronic interactions between the ZnBC subunits in alkyne-linked arrays is strongly dependent on the dihedral angle between the ZnBC subunits, with coplanar and perpendicular conformations resulting in the largest and smallest amount of the electronic interactions, respectively. This creates the potential for several stable conformations of the arrays with very different ground and excited state properties.

ZnBC oligomers in general display similar amounts of electronic interactions among the ZnBC subunits as their respective dimers. Strongly interacting oligomers exhibit a significant decrease in the HOMO−LUMO gap and show an increase in the orbital energy dispersion as the array size increases The HOMO−LUMO gap of weakly interacting arrays displays only a minimal decrease with the increase of the array size, and the frontier MO region is characterized by the high degree of degeneracy.

In conclusion, we have shown that the strength of electronic interactions among the bacteriochlorin subunits can be tuned both by the choice of the linker and linker attachment site. It is apparent from the analysis of the ground state electronic structure that the linker, linker attachment site, and size of the array will all have repercussions for their excited state properties. Further studies on the excited state properties of these arrays are necessary to better understand the effects of these repercussions on the electronic absorption spectra of ZnBC molecular arrays.

■ ASSOCIATED CONTENT

Supporting Information

Figures of the molecular structures of ZnBC dimers and oligomers, energy level diagrams of the frontier orbitals of ZnBC dimers at their ground state structures, PES scans with respect to rotation about select bonds in ZnBC dimers, frontier orbital energies and frontier orbital populations densities on linker atoms in ZnBC dimers at various points of their PESs, fragmentation scheme for *meso*-ethynyl trimer, and a table of imaginary frequencies at optimized structures of ZnBC oligomers. This material is available free of charge via the Internet at http://pubs.acs.org.

■ AUTHOR INFORMATION

Corresponding Author

*E-mail: ejakubi@ncsu.edu.

Notes

The authors declare no competing financial interest.

■ ACKNOWLEDGMENTS

This work was supported by the Department of Chemistry at North Carolina State University (NCSU) and used the Extreme Science and Engineering Discovery Environment (XSEDE) through the National Science Foundation Grant TG-CHE120019. J.M.G.D. acknowledges the NCSU Department of Chemistry Summer Internship Program. We also thank Dr. Jonathan S. Lindsey for helpful discussions.

■ REFERENCES

(1) Collins, A. M.; Qian, P.; Tang, Q.; Bocian, D. F.; Hunter, C. N.; Blankenship, R. E. Light-Harvesting Antenna System from the Phototrophic Bacterium Roseiflexus Castenholzii. *Biochemistry* **2010**, *49*, 7524−7531.

(2) Boxer, S. G. Model Reactions in Photosynthesis. *Biochim. Biophys. Acta, Rev. Bioenerg.* **1983**, *726*, 265−292.

(3) Scheer, H. An Overview of Chlorophylls and Bacteriochlorophylls: Biochemistry, Biophysics, Functions and Applications. In *Chrophylls and Bacteriochlorophylls Biochemistry, Biophysics, Functions and Applications (Advances in Photosynthesis and Respiration)*; Grimm, B.; PorraR. J. , Rudiger, W.; Scheer, H., Eds.; Springer: Dordrecht, The Netherlands, 2006; Vol. *25*, pp 1−26.
(4) Hanson, L. K. Theoretical Calculations of Photosynthetic Pigments. *Photochem. Photobiol.* **1988**, *47*, 903−921.
(5) *Near-Infrared Dyes for High Technology Applications*; Daehne, S., Resch-Genger, U., Wolfbeis, O. S., Eds.; Springer: Dordrecht, The Netherlands, 1998.
(6) Gust, D.; Moore, T. A.; Moore, A. L. Molecular Mimicry of Photosynthetic Energy and Electron Transfer. *Acc. Chem. Res.* **1993**, *26*, 198−205.
(7) Hasselman, G. M.; Watson, D. F.; Stromberg, J. R.; Bocian, D. F.; Holten, D.; Lindsey, J. S.; Meyer, G. J. Theoretical Solar-to-Electrical Energy-Conversion Efficiencies of Perylene-Porphyrin Light-Harvesting Arrays. *J. Phys. Chem. B* **2006**, *110*, 25430−25440.
(8) Yang, J.; Yoon, M. C.; Yoo, H.; Kim, P.; Kim, D. Excitation Energy Transfer in Multiporphyrin Arrays with Cyclic Architectures: Towards Artificial Light-Harvesting Antenna Complexes. *Chem. Soc. Rev.* **2012**, *41*, 4808−4826.
(9) Duan, X.; Huang, Y.; Lieber, C. M. Nonvolatile Memory and Programmable Logic from Molecule-Gated Nanowires. *Nano Lett.* **2002**, *2*, 487−490.
(10) Kwok, K. S.; Ellenbogen, J. C. Moletronics: Future Electronics. *Mater. Today* **2002**, *5*, 28−37.
(11) Hindin, E.; Forties, R. A.; Loewe, R. S.; Ambroise, A.; Kirmaier, C.; Bocian, D. F.; Lindsey, J. S.; Holten, D.; Knox, R. S. Excited-State Energy Flow in Covalently Linked Multiporphyrin Arrays: The Essential Contribution of Energy Transfer between Nonadjacent Chromophores. *J. Phys. Chem. B* **2004**, *108*, 12821−12832.
(12) Holten, D.; Bocian, D. F.; Lindsey, J. S. Probing Electronic Communication in Covalently Linked Multiporphyrin Arrays. A Guide to the Rational Design of Molecular Photonic Devices. *Acc. Chem. Res.* **2002**, *35*, 57−69.
(13) Van Patten, P. G.; Shreve, A. P.; Lindsey, J. S.; Donohoe, R. J. Energy-Transfer Modeling for the Rational Design of Multiporphyrin Light-Harvesting Arrays. *J. Phys. Chem. B* **1998**, *102*, 4209−4216.
(14) Sprafke, J. K.; Kondratuk, D. V.; Wykes, M.; Thompson, A. L.; Hoffmann, M.; Drevinskas, R.; Chen, W. H.; Yong, C. K.; Karnbratt, J.; Bullock, J. E.; et al. Belt-Shaped Pi-Systems: Relating Geometry to Electronic Structure in a Six-Porphyrin Nanoring. *J. Am. Chem. Soc.* **2011**, *133*, 17262−17273.
(15) Seth, J.; Palaniappan, V.; Johnson, T. E.; Prathapan, S.; Lindsey, J. S.; Bocian, D. F. Investigation of Electronic Communication in Multi-Porphyrin Light-Harvesting Arrays. *J. Am. Chem. Soc.* **1994**, *116*, 10578−10592.
(16) Gouterman, M. Optical Spectra and Electronic Structure of Porphyrins and Related Rings. In *The Porphyrins*; Dolphin, D., Ed.; Academic Press: New York, 1978; Vol. *3*, pp 1−165.
(17) Stromberg, J. R.; Marton, A.; Kee, H. L.; Kirmaier, C.; Diers, J. R.; Muthiah, C.; Taniguchi, M.; Lindsey, J. S.; Bocian, D. F.; Meyer, G. J.; et al. Examination of Tethered Porphyrin, Chlorin, and Bacteriochlorin Molecules in Mesoporous Metal-Oxide Solar Cells. *J. Phys. Chem. C* **2007**, *111*, 15464−15478.
(18) Lindsey, J. S.; Mass, O.; Chen, C.-Y. Tapping the near-Infrared Spectral Region with Bacteriochlorin Arrays. *New J. Chem.* **2011**, *35*, 511.
(19) Kobayashi, R.; Amos, R. D. The Application of Cam-B3lyp to the Charge-Transfer Band Problem of the Zincbacteriochlorin−Bacteriochlorin Complex. *Chem. Phys. Lett.* **2006**, *420*, 106−109.
(20) Vasudevan, J.; Stibrany, R. T.; Bumby, J.; Knapp, S.; Potenza, J. A.; Emge, T. J.; Schugar, H. J. An Edge-over-Edge Zn(II) Bacteriochlorin Dimer Having an Unshifted Qy band. The Importance of Π-Overlap. *J. Am. Chem. Soc.* **1996**, *118*, 11676−11677.
(21) Dreuw, A.; Head-Gordon, M. Failure of Time-Dependent Density Functional Theory for Long-Range Charge-Transfer Excited States: The Zincbacteriochlorin-Bacteriochlorin and Bacteriochlorophyll-Spheroidene Complexes. *J. Am. Chem. Soc.* **2004**, *126*, 4007−4016.
(22) Wasielewski, M. R.; Svec, W. A. Synthesis of Covalently Linked Dimeric Derivatives of Chlorophyll a, Pyrochlorophyll a, Chlorophyll B, and Bacteriochlorophyll A. *J. Org. Chem.* **1980**, *45*, 1969−1974.
(23) Wasielewski, M. R.; Smith, U. H.; Cope, B. T.; Katz, J. J. A Synthetic Biomimetic Model of Special Pair Bacteriochlorophyll A. *J. Am. Chem. Soc.* **1977**, *99*, 4172−4173.
(24) Muthiah, C.; Kee, H. L.; Diers, J. R.; Fan, D.; Ptaszek, M.; Bocian, D. F.; Holten, D.; Lindsey, J. S. Synthesis and Excited-State Photodynamics of a Chlorin-Bacteriochlorin Dyad–through-Space Versus through-Bond Energy Transfer in Tetrapyrrole Arrays. *Photochem. Photobiol.* **2008**, *84*, 786−801.
(25) Kee, H. L.; Diers, J. R.; Ptaszek, M.; Muthiah, C.; Fan, D.; Lindsey, J. S.; Bocian, D. F.; Holten, D. Chlorin-Bacteriochlorin Energy-Transfer Dyads as Prototypes for Near-Infrared Molecular Imaging Probes: Controlling Charge-Transfer and Fluorescence Properties in Polar Media. *Photochem. Photobiol.* **2009**, *85*, 909−920.
(26) Kee, H. L.; Nothdurft, R.; Muthiah, C.; Diers, J. R.; Fan, D.; Ptaszek, M.; Bocian, D. F.; Lindsey, J. S.; Culver, J. P.; Holten, D. Examination of Chlorin-Bacteriochlorin Energy-Transfer Dyads as Prototypes for near-Infrared Molecular Imaging Probes. *Photochem. Photobiol.* **2008**, *84*, 1061−1072.
(27) Kim, H. J.; Lindsey, J. S. De Novo Synthesis of Stable Tetrahydroporphyrinic Macrocycles: Bacteriochlorins and a Tetradehydrocorrin. *J. Org. Chem.* **2005**, *70*, 5475−5486.
(28) Taniguchi, M.; Cramer, D. L.; Bhise, A. D.; Kee, H. L.; Bocian, D. F.; Holten, D.; Lindsey, J. S. Accessing the Near-Infrared Spectral Region with Stable, Synthetic, Wavelength-Tunable Bacteriochlorins. *New J. Chem.* **2008**, *32*, 947−958.
(29) Yu, Z.; Ptaszek, M. Near-IR Emissive Chlorin-Bacteriochlorin Energy-Transfer Dyads with a Common Donor and Acceptors with Tunable Emission Wavelength. *J. Org. Chem.* **2013**, *78*, 10678−10691.
(30) Osuka, A.; Wada, Y.; Maruyama, K.; Tamiaki, H. Synthesis of a Covalently Linked Bacteriopyropheophorbide—Pyropheophorbide Hybrid Dimer. *Heterocycles* **1997**, *44*, 165−168.
(31) Tamiaki, H.; Miyatake, T.; Tanikaga, R.; Holzwarth, A. R.; Schaffner, K. Self-Assembly of an Artificial Light-Harvesting Antenna: Energy Transfer from a Zinc Chlorin to a Bacteriochlorin in a Supramolecular Aggregate. *Angew. Chem., Int. Ed. Engl.* **1996**, *35*, 772−774.
(32) Miyatake, T.; Tamiaki, H.; Holzwarth, A. R.; Schaffner, K. Artificial Light-Harvesting Antennae: Singlet Excitation Energy Transfer from Zinc Chlorin Aggregate to Bacteriochlorin in Homogeneous Hexane Solution. *Photochem. Photobiol.* **1999**, *69*, 448−456.
(33) Prokhorenko, V. I.; Holzwarth, A. R.; Müller, M. G.; Schaffner, K.; Miyatake, T.; Tamiaki, H. Energy Transfer in Supramolecular Artificial Antennae Units of Synthetic Zinc Chlorins and Co-Aggregated Energy Traps. A Time-Resolved Fluorescence Study†,‡. *J. Phys. Chem. B* **2002**, *106*, 5761−5768.
(34) Grin, M. A.; Lonin, I. S.; Fedyunin, S. V.; Tsiprovskiy, A. G.; Strizhakov, A. A.; Tsygankov, A. A.; Krasnovsky, A. A.; Mironov, A. F. Synthesis and Properties of the Zn-Chlorin−Bacteriochlorin Dimer. *Mendeleev Commun.* **2007**, *17*, 209−211.
(35) Petit, L.; Quartarolo, A.; Adamo, C.; Russo, N. Spectroscopic Properties of Porphyrin-Like Photosensitizers: Insights from Theory. *J. Phys. Chem. B* **2006**, *110*, 2398−2404.
(36) Petit, L.; Adamo, C.; Russo, N. Absorption Spectra of First-Row Transition Metal Complexes of Bacteriochlorins: A Theoretical Analysis. *J. Phys. Chem. B* **2005**, *109*, 12214−12221.
(37) Tsai, H.-H.; Simpson, M. C. The Role of Frontier Molecular Orbital Ordering on Electronic Communication in Porphyrin Arrays. *Chem. Phys. Lett.* **2002**, *353*, 111−118.
(38) Wilson, G. J.; Arnold, D. P. Time-Dependent Density Functional Molecular Orbital and Excited State Calculations on Bis(Porphyrinyl)Butadiynes in the Monocationic, Neutral, Monoanionic, and Dianionic Oxidation States. *J. Phys. Chem. A* **2005**, *109*, 6104−6113.

(39) Yamaguchi, Y.; Yokomichi, Y.; Yokoyama, S.; Mashiko, S. Time-Dependent Density Functional Calculations of the Q-Like Bands of Phenylene-Linked Free-Base and Zinc Porphyrin Dimers. *Int. J. Quantum Chem.* **2001**, *84*, 338−347.
(40) Hamamura, T.; Dy, J. T.; Tamaki, K.; Nakazaki, J.; Uchida, S.; Kubo, T.; Segawa, H. Dye-Sensitized Solar Cells Using Ethynyl-Linked Porphyrin Trimers. *Phys. Chem. Chem. Phys.* **2014**, *16*, 4551−4560.
(41) Stranger, R.; McGrady, J. E.; Arnold, D. P.; Lane, I.; Heath, G. A. Communication between Porphyrin Rings in the Butadiyne-Bridged Dimer Ni(Oep)(M-C4)Ni(Oep): A Density Functional Study. *Inorg. Chem.* **1996**, *35*, 7791−7797.
(42) Miyahara, T.; Nakatsuji, H.; Hasegawa, J.; Osuka, A.; Aratani, N.; Tsuda, A. Ground and Excited States of Linked and Fused Zinc Porphyrin Dimers: Symmetry Adapted Cluster (Sac)—Configuration Interaction (CI) Study. *J. Chem. Phys.* **2002**, *117*, 11196−11207.
(43) Nakai, K.; Sahnoun, R.; Kato, T.; Kono, H.; Fujimura, Y. Time-Dependent Density Functional Theory Investigation of Electric Field Effects on Absorption Spectra of Meso-Meso-Linked Zinc Porphyrin Arrays: Role of Charge-Transfer States. *J. Phys. Chem. B* **2005**, *109*, 13921−13927.
(44) Kuter, D.; Venter, G. A.; Naidoo, K. J.; Egan, T. J. Experimental and Time-Dependent Density Functional Theory Characterization of the Uv-Visible Spectra of Monomeric and Mu-Oxo Dimeric Ferriprotoporphyrin IX. *Inorg. Chem.* **2012**, *51*, 10233−10250.
(45) Petke, J. D.; Maggiora, G. M. Quantum Mechanical Studies of Charge-Transfer States in Porphyrin Heterodimers. In *Porphyrins*; ACS Symposium Series; American Chemical Society: Washington, D.C., 1986; Vol. *321*, pp 20−50.
(46) Okuno, Y.; Kamikado, T.; Yokoyama, S.; Mashiko, S. Determining the Conformation of a Phenylene-Linked Porphyrin Dimer by NMR Spectroscopy and Quantum Chemical Calculations. *J. Mol. Struct.: THEOCHEM* **2003**, *631*, 13−20.
(47) Okuno, Y.; Kamikado, T.; Yokoyama, S.; Mashiko, S. Theoretical Study of Aryl-Ring Rotation in Arylporphyrins. *J. Mol. Struct.: THEOCHEM* **2002**, *594*, 55−60.
(48) Susumu, K.; Maruyama, H.; Kobayashi, H.; Tanaka, K. Theoretical Approach to the Design of Supramolecular Conjugated Porphyrin Polymers. *J. Mater. Chem.* **2001**, *11*, 2262−2270.
(49) Ohira, S.; Brédas, J.-L. Porphyrin Dimers: A Theoretical Understanding of the Impact of Electronic Coupling Strength on the Two-Photon Absorption Properties. *J. Mater. Chem.* **2009**, *19*, 7545−7550.
(50) Okuno, Y.; Mashiko, S. Theoretical Investigation of Excitation Energy Transfer Mechanism in Porphyrin Dimeric Array. *Jpn. J. Appl. Phys.* **2006**, *45*, 475−478.
(51) Okuno, Y.; Mashiko, S. Theoretical Study of Excitation-Energy Transfer in a Diarylethyne-Linked Porphyrin Array. *Thin Solid Films* **2003**, *438*−*439*, 215−220.
(52) Okuno, Y.; Mashiko, S. Convenient Expression of the Rate Constant for Nonadiabatic Transition. *Int. J. Quantum Chem.* **2005**, *102*, 8−18.
(53) Okuno, Y.; Mashiko, S. Theory of Excitation Energy Transfer Regarded as Nonadiabatic Transition 2: Calculational Evidence of Nonadiabatic Interaction Causing Intermolecular Excitation Energy Transfer. *Int. J. Quantum Chem.* **2003**, *94*, 36−43.
(54) Okuno, Y.; Mashiko, S. A Theory of Excitation-Energy Transfer Regarded as Nonadiabatic Transition and Its Comparison to Forster's Theory. *Int. J. Quantum Chem.* **2002**, *90*, 772−777.
(55) Thompson, M. A.; Zerner, M. C.; Fajer, J. Electronic Structure of Bacteriochlorophyll Dimers. 1. Bacteriochlorin Models. *J. Phys. Chem.* **1990**, *94*, 3820−3828.
(56) Duchemin, I.; Deutsch, T.; Blase, X. Short-Range to Long-Range Charge-Transfer Excitations in the Zincbacteriochlorin-Bacteriochlorin Complex: A Bethe-Salpeter Study. *Phys. Rev. Lett.* **2012**, *109*, 167801-1−167801-5.
(57) Yanai, T.; Tew, D. P.; Handy, N. C. A New Hybrid Exchange−Correlation Functional Using the Coulomb-Attenuating Method (Cam-B3lyp). *Chem. Phys. Lett.* **2004**, *393*, 51−57.
(58) Tsuchiya, T.; Shrestha, K.; Jakubikova, E. Orbital Analysis and Excited-State Calculations in an Energy-Based Fragmentation Method. *J. Chem. Theory Comput.* **2013**, *9*, 3350−3363.
(59) Scholes, G. D. Long-Range Resonance Energy Transfer in Molecular Systems. *Annu. Rev. Phys. Chem.* **2003**, *54*, 57−87.
(60) Albinsson, B.; Martensson, J. Excitation Energy Transfer in Donor-Bridge-Acceptor Systems. *Phys. Chem. Chem. Phys.* **2010**, *12*, 7338−7351.
(61) Oevering, H.; Verhoeven, J. W.; Paddon-Row, M. N.; Cotsaris, E.; Hush, N. S. Long-Range Exchange Contribution to Singlet-Singlet Energy Transfer in a Series of Rigid Bichromophoric Molecules. *Chem. Phys. Lett.* **1988**, *143*, 488−495.
(62) Caprasecca, S.; Mennucci, B. Excitation Energy Transfer in Donor-Bridge-Acceptor Systems: A Combined Quantum-Mechanical/Classical Analysis of the Role of the Bridge and the Solvent. *J. Phys. Chem. A* **2014**, *118*, 6484−6491.
(63) Eng, M. P.; Ljungdahl, T.; Martensson, J.; Albinsson, B. Triplet Excitation Energy Transfer in Porphyrin-Based Donor–Bridge–Acceptor Systems with Conjugated Bridges of Varying Length: An Experimental and DFT Study. *J. Phys. Chem. B* **2006**, *110*, 6483−6491.
(64) Asano, M. S.; Yamashita, K.; Kitabayashi, M.; Kusama, K.; Kagota, D.; Sugiura, K. Superexchange Mediated Energy Transfer in Zinc(II) Porphyrin-Free Base Porphyrin Dimers: Comparison of M- and P-Bis(Phenylethynyl) Phenylene Linked Dimers. *Phys. Chem. Chem. Phys.* **2011**, *13*, 12712−12715.
(65) Pettersson, K.; Kyrychenko, A.; Ronnow, E.; Ljungdahl, T.; Martensson, J.; Albinsson, B. Singlet Energy Transfer in Porphyrin-Based Donor-Bridge-Acceptor Systems: Interaction between Bridge Length and Bridge Energy. *J. Phys. Chem. A* **2006**, *110*, 310−318.
(66) Curutchet, C.; Feist, F. A.; Van Averbeke, B.; Mennucci, B.; Jacob, J.; Mullen, K.; Basche, T.; Beljonne, D. Superexchange-Mediated Electronic Energy Transfer in a Model Dyad. *Phys. Chem. Chem. Phys.* **2010**, *12*, 7378−7385.
(67) Song, H. E.; Taniguchi, M.; Diers, J. R.; Kirmaier, C.; Bocian, D. F.; Lindsey, J. S.; Holten, D. Linker Dependence of Energy and Hole Transfer in Neutral and Oxidized Multiporphyrin Arrays. *J. Phys. Chem. B* **2009**, *113*, 16483−16493.
(68) Kilså, K.; Kajanus, J.; Mårtensson, J.; Albinsson, B. Mediated Electronic Coupling: Singlet Energy Transfer in Porphyrin Dimers Enhanced by the Bridging Chromophore. *J. Phys. Chem. B* **1999**, *103*, 7329−7339.
(69) Haser, M.; Almlof, J. Laplace Transform Techniques in Møller–Plesset Perturbation Theory. *J. Chem. Phys.* **1992**, *96*, 489−494.
(70) Yang, W. A Local Projection Method for the Linear Combination of Atomic Orbital Implementation of Density-Functional Theory. *J. Chem. Phys.* **1991**, *94*, 1208−1214.
(71) Friesner, R. A.; Murphy, R. B.; Beachy, M. D.; Ringnalda, M. N.; Pollard, W. T.; Dunietz, B. D.; Cao, Y. Correlated Ab Initio Electronic Structure Calculations for Large Molecules. *J. Phys. Chem. A* **1999**, *103*, 1913−1928.
(72) Wu, S. Y.; Jayanthi, C. S. Order-N Methodologies and Their Applications. *Phys. Rep.* **2002**, *358*, 1−74.
(73) Saebo, S.; Pulay, P. Local Treatment of Electron Correlation. *Annu. Rev. Phys. Chem.* **1993**, *44*, 213−236.
(74) Humbel, S.; Sieber, S.; Morokuma, K. The IMOMO Method: Integration of Different Levels of Molecular Orbital Approximations for Geometry Optimization of Large Systems: Test for N-Butane Conformation and SN2 Reaction: RCl+Cl−. *J. Chem. Phys.* **1996**, *105*, 1959−1967.
(75) Svensson, M.; Humbel, S.; Froese, R. D. J.; Matsubara, T.; Sieber, S.; Morokuma, K. Oniom: A Multilayered Integrated Mo + Mm Method for Geometry Optimizations and Single Point Energy Predictions. A Test for Diels−Alder Reactions and Pt(P(T-Bu)3)2 + H2 Oxidative Addition. *J. Phys. Chem.* **1996**, *100*, 19357−19363.
(76) Senn, H. M.; Thiel, W. QM/MM Methods for Biomolecular Systems. *Angew. Chem., Int. Ed.* **2009**, *48*, 1198−1229.
(77) Neugebauer, J.; Curutchet, C.; Muñoz-Losa, A.; Mennucci, B. A Subsystem Tddft Approach for Solvent Screening Effects on Excitation

Energy Transfer Couplings. *J. Chem. Theory Comput.* **2010**, *6*, 1843−1851.
(78) Hofener, S.; Gomes, A. S.; Visscher, L. Molecular Properties Via a Subsystem Density Functional Theory Formulation: A Common Framework for Electronic Embedding. *J. Chem. Phys.* **2012**, *136*, 044104-1−044104-16.
(79) Gordon, M. S.; Fedorov, D. G.; Pruitt, S. R.; Slipchenko, L. V. Fragmentation Methods: A Route to Accurate Calculations on Large Systems. *Chem. Rev.* **2012**, *112*, 632−672.
(80) Exner, T. E.; Mezey, P. G. Ab Initio-Quality Electrostatic Potentials for Proteins: An Application of the Adma Approach. *J. Phys. Chem. A* **2002**, *106*, 11791−11800.
(81) Fujimoto, K.; Yang, W. Density-Fragment Interaction Approach for Quantum-Mechanical/Molecular-Mechanical Calculations with Application to the Excited States of a Mg^{2+}-Sensitive Dye. *J. Chem. Phys.* **2008**, *129*, 054102−054110.
(82) Imamura, A.; Aoki, Y.; Maekawa, K. A Theoretical Synthesis of Polymers by Using Uniform Localization of Molecular Orbitals: Proposal of an Elongation Method. *J. Chem. Phys.* **1991**, *95*, 5419−5431.
(83) Yang, W.; Lee, T.-S. A Density-Matrix Divide-and-Conquer Approach for Electronic Structure Calculations of Large Molecules. *J. Chem. Phys.* **1995**, *103*, 5674−5678.
(84) Ganesh, V.; Dongare, R. K.; Balanarayan, P.; Gadre, S. R. Molecular Tailoring Approach for Geometry Optimization of Large Molecules: Energy Evaluation and Parallelization Strategies. *J. Chem. Phys.* **2006**, *125*, 104109-1−104109-10.
(85) Fedorov, D. G.; Nagata, T.; Kitaura, K. Exploring Chemistry with the Fragment Molecular Orbital Method. *Phys. Chem. Chem. Phys.* **2012**, *14*, 7562−7577.
(86) Huang, L.; Bohorquez, H. J.; Matta, C. F.; Massa, L. The Kernel Energy Method: Application to Graphene and Extended Aromatics. *Int. J. Quantum Chem.* **2011**, *111*, 4150−4157.
(87) Hua, S.; Hua, W.; Li, S. An Efficient Implementation of the Generalized Energy-Based Fragmentation Approach for General Large Molecules. *J. Phys. Chem. A* **2010**, *114*, 8126−8134.
(88) Deev, V.; Collins, M. A. Approximate Ab Initio Energies by Systematic Molecular Fragmentation. *J. Chem. Phys.* **2005**, *122*, 154102-1−154102-12.
(89) Li, W.; Li, S.; Jiang, Y. Generalized Energy-Based Fragmentation Approach for Computing the Ground-State Energies and Properties of Large Molecules. *J. Phys. Chem. A* **2007**, *111*, 2193−2199.
(90) Becke, A. D. Density-Functional Thermochemistry. III. The Role of Exact Exchange. *J. Chem. Phys.* **1993**, *98*, 5648−5652.
(91) Stephens, P. J.; Devlin, F. J.; Chabalowski, C. F.; Frisch, M. J. Ab-Initio Calculation of Vibrational Absorption and Circular-Dichroism Spectra Using Density Functional Force Fields. *J. Phys. Chem.* **1994**, *98*, 11623−11627.
(92) Hehre, W. J.; Ditchfield, R.; Pople, J. A. Self-Consistent Molecular Orbital Methods. XII. Further Extensions of Gaussian-Type Basis Sets for Use in Molecular Orbital Studies of Organic Molecules. *J. Chem. Phys.* **1972**, *56*, 2257−2261.
(93) Harihara, P. C.; Pople, J. A. The Influence of Polarization Functions on Molecular Orbital Hydrogenation Energies. *Theor. Chim. Acta* **1973**, *28*, 213−222.
(94) Roy, L. A.; Hay, P. J.; Martin, R. L. Revised Sets for Transition Metal Atoms Using the Lanl Effective Core Potentials. *J. Chem. Theory Comput.* **2008**, *4*, 1029−1031.
(95) Frisch, M. J.; Trucks, G. W.; Schlegel, H. B.; Scuseria, G. E.; Robb, M. A.; Cheeseman, J. R.; Scalmani, G.; Barone, V.; Mennucci, B.; Petersson, G. A.; et al. *Gaussian 09*, revision B.01; Gaussian Inc.: Wallingford, CT, 2009.
(96) Dennington, R.; Keith, T.; Millam, J. *Gaussview*, version 5; Semichem Inc.: Shawnee Mission, KS, 2009.
(97) Babu, K.; Ganesh, V.; Gadre, S. R.; Ghermani, N. E. Tailoring Approach for Exploring Electron Densities and Electrostatic Potentials of Molecular Crystals. *Theor. Chem. Acc.* **2004**, *111*, 255−263.
(98) Bettens, R. P. A.; Lee, A. M. A New Algorithm for Molecular Fragmentation in Quantum Chemical Calculations. *J. Phys. Chem. A* **2006**, *110*, 8777−8785.
(99) He, X.; Zhang, J. Z. A New Method for Direct Calculation of Total Energy of Protein. *J. Chem. Phys.* **2005**, *122*, 31103-1−31103-4.
(100) Hua, W. J.; Fang, T.; Li, W.; Yu, J. G.; Li, S. H. Geometry Optimizations and Vibrational Spectra of Large Molecules from a Generalized Energy-Based Fragmentation Approach. *J. Phys. Chem. A* **2008**, *112*, 10864−10872.
(101) Vukmirovic, N.; Wang, L. W. Overlapping Fragments Method for Electronic Structure Calculation of Large Systems. *J. Chem. Phys.* **2011**, *134*, 094119-1−094119-8.
(102) Zhang, D. W.; Zhang, J. Z. H. Molecular Fractionation with Conjugate Caps for Full Quantum Mechanical Calculation of Protein-Molecule Interaction Energy. *J. Chem. Phys.* **2003**, *119*, 3599−3605.
(103) Zhengji, Z.; et al. A Divide-and-Conquer Linear Scaling Three-Dimensional Fragment Method for Large Scale Electronic Structure Calculations. *J. Phys.: Condens. Matter* **2008**, *20*, 294203-1−294203-8.
(104) Schlegel, H. B. Geometry Optimization. *Wiley Interdiscip. Rev.: Comput. Mol. Sci.* **2011**, *1*, 790−809.
(105) Gouterman, M.; Wagnière, G. H.; Snyder, L. C. Spectra of Porphyrins. *J. Mol. Spectrosc.* **1963**, *11*, 108−127.
(106) Gouterman, M. Spectra of Porphyrins. *J. Mol. Spectrosc.* **1961**, *6*, 138−163.
(107) Canadell, E.; Whangbo, M. H. Conceptual Aspects of Structure-Property Correlations and Electronic Instabilities, with Applications to Low-Dimensional Transition-Metal Oxides. *Chem. Rev. (Washington, DC, U.S.)* **1991**, *91*, 965−1034.
(108) Tsuchiya, T.; Jakubikova, E. Role of Noncoplanar Conformation in Facilitating Ground State Hole Transfer in Oxidized Porphyrin Dyads. *J. Phys. Chem. A* **2012**, *116*, 10107−10114.
(109) Ambroise, A.; Kirmaier, C.; Wagner, R. W.; Loewe, R. S.; Bocian, D. F.; Holten, D.; Lindsey, J. S. Weakly Coupled Molecular Photonic Wires: Synthesis and Excited-State Energy-Transfer Dynamics. *J. Org. Chem.* **2002**, *67*, 3811−3826.
(110) Wagner, R. W.; Lindsey, J. S.; Seth, J.; Palaniappan, V.; Bocian, D. F. Molecular Optoelectronic Gates. *J. Am. Chem. Soc.* **1996**, *118*, 3996−3997.
(111) Lin, V. S. Y.; Therien, M. J. The Role of Porphyrin-to-Porphyrin Linkage Topology in the Extensive Modulation of the Absorptive and Emissive Properties of a Series of Ethynyl- and Butadiynyl-Bridged Bis- and Tris(Porphinato)Zinc Chromophores. *Chem.−Eur. J.* **1995**, *1*, 645−651.
(112) Kumble, R.; Palese, S.; Lin, V. S. Y.; Therien, M. J.; Hochstrasser, R. M. Ultrafast Dynamics of Highly Conjugated Porphyrin Arrays. *J. Am. Chem. Soc.* **1998**, *120*, 11489−11498.
(113) Winters, M. U.; Karnbratt, J.; Eng, M.; Wilson, C. J.; Anderson, H. L.; Albinsson, B. Photophysics of a Butadiyne-Linked Porphyrin Dimer: Influence of Conformational Flexibility in the Ground and First Singlet Excited State. *J. Phys. Chem. C* **2007**, *111*, 7192−7199.